Supporting Information for

Construction of clay-mediated nZVI composites to alleviate the decline in Cr(VI) removal during co-transport with humic acid and phosphate

Wenxin Jiang [a], Nan Xu [a,*], Wu Sun [a], Feng Du [b]

[a] School of Environmental Science and Engineering, Suzhou University of Science and Technology, Suzhou 215009, China

[b] School of Materials Science and Engineering, Suzhou University of Science and Technology, Suzhou 215009, China

*Corresponding Authors: Dr. Nan Xu, E-mail: nanxu@mail.usts.edu.cn

24 Pages; 5 Tables; and 11 Figures

TABLE OF CONTENTS	Pages
Text S1: Chemicals and reagents	1
Text S2: Synthesis of clay-mediated nZVI@GT composites	1
Text S3: Measurement of Cr and Fe concentration	2
Text S4: Pretreatment of column transport experiment	3
Text S5: Two-site kinetic attachment model	4
Text S6: Characterization of synthesized M-nZVI@GT and K-nZVI@GT	4
References	6
Table S1. Transport percentage of different Cr species in the effluent when M-nZVI@GT and K-nZVI@GT cotransport with Cr(VI) in the presence of phosphate or HA.	9
Table S2. Mass recovery of total Fe and total Cr in the effluent and sand columns during transport of M-nZVI@GT and K-nZVI@GT with Cr(VI) under different experimental conditions.	10
Table S3. Components and corresponding relative percentage of Fe 2p and Cr 2p XPS spectra for M-nZVI@GT and K-nZVI@GT after reaction with Cr(VI) in the presence of phosphate or HA.	11
Table S4. Removal capacity of Cr(VI) by different types of nZVI nanocomposites.	**12**
Table S5. Estimated cost for the clay-mediated nZVI@GT material.	13
Fig. S1. Experimental set-up diagrams for batch (a) and column transport experiment (b).	14
Fig. S2. SEM images of Mont (a), M-nZVI@GT (b), Kaolin (d), K-nZVI@GT (e), and EDS of M-nZVI@GT (c) and K-nZVI@GT (f).	15
Fig. S3. XRD patterns (a, b) and FTIR spectra (c, d) of Mont, M-nZVI@GT, Kaolin and K-nZVI@GT.	16
Fig. S4. FTIR spectra of M-nZVI@GT (a) and K-nZVI@GT (b) in the presence of phosphate and HA.	17
Fig. S5. XPS full scan spectra of M-nZVI@GT (a) and K-nZVI@GT (b) with Cr(VI) in the presence of phosphate and HA.	18
Fig. S6. BET of M-nZVI@GT (a) and K-nZVI@GT (b).	19

Fig. S7. Cr(VI) removal efficiency of M-nZVI@GT (a) and K-nZVI@GT (b) over time in the presence of phosphate and HA at pH 3.0.	20
Fig. S8. Retention profiles of M-nZVI@GT (a, b, c) and K-nZVI@GT (d, e, f) (0.5 g·L^{-1}) cotransport with Cr(VI) (50 mg·L^{-1}) in the presence of phosphate (b, e) and HA (c, f) in 1 mM NaCl solution at pH 6.0.	21
Fig. S9. Suspension kinetics of nZVI@GT, M-nZVI@GT and K-nZVI@GT in 1 mM NaCl at pH 6.0.	22
Fig. S10. Correlation between k_{1d}/k_1 values and transport mass recovery of Fe (a) and correlation between k_2 values and retention mass recovery of Fe (b) for clay modified nZVI@GT composites in the presence of phosphate and HA.	23
Fig. S11. Recycling for the Cr(VI) removal efficiency of M-nZVI@GT (a) and K-nZVI@GT (b) (0.5 g L^{-1}) in the presence of phosphate and HA at pH 3.0.	24

Additional materials and methods

Text S1: Chemicals and reagents

The green tea was purchased from Beijing Qiyuan Xianshan Tea Co., Ltd. The chemicals (including Mont, Kaolin, sodium dihydrogen phosphate (NaH_2PO_4), and HA) with a purity of 99% were supplied by Aladdin Reagent Co., Ltd. Hydrated ferric sulfate ($Fe_2(SO_4)_3 \cdot 7H_2O$), potassium dichromate ($K_2Cr_2O_7$), and diphenylcarbazide were provided by Sinopharm Chemical Reagent Corporation. Cr and Fe standard solutions were purchased from AccuStandard and Aladdin Reagent Co., Ltd., respectively.

Text S2: Synthesis of clay-mediated nZVI@GT composites

In the previous synthesis, tea polyphenols (TPs) were extracted from green tea as reducing agents. The TPs contained 161-195 $mg \cdot g^{-1}$ catechins.[1] Following the synthetic methods from our previous studies,[2] we synthesized clay-mediated nZVI@GT materials (including M-nZVI@GT and K-nZVI@GT). Clays (Montmorillonite and Kaolin) and $Fe_2(SO_4)_3$ solution were pre-mixed in a 10:1 mass ratio for 24 hours to introduce iron ions into the clay structure. The resulting mixture was then reacted with green tea extract in a four-necked flask using a bottom-up method.[3, 4]Green tea extract acted as a reducing agent to reduce Fe^{3+}/Fe^{3+} to Fe^0. The mixture was stirred at 300 rpm under a nitrogen atmosphere for 30 minutes. After centrifugation (4000 rpm, 7 min), the precipitate was washed several times with anhydrous ethanol and dried under vacuum (60°C, -70 cm Hg). The obtained M-nZVI@GT and K-nZVI@GT were ground and passed through a 200-mesh sieve before being prepared for use, with an iron content of about 8%. The successful preparation of the materials was confirmed by SEM (Fig. S2) and XRD patterns (Fig. S3). As seen in Table S5, the green synthesis method for clay-mediated nZVI@GT composites is more cost-effective, with a cost of ¥ 7.85/g, which is significantly lower than the chemical method.

Text S3: Measurement of Cr and Fe concentration

The study quantified the removal of Cr(VI) by clay-mediated nZVI@GT composites in terms of particulate Cr (adsorption) and soluble Cr(III) (reduction). Particulate Cr was defined as Cr(III)/Cr(VI) adsorbed on composites and Cr(III) precipitation. Flame atomic absorption spectrometry (FAAS) was used to determine the concentrations of total Cr (after acid digestion) and total soluble Cr, following the USEPA 7196A method. The Cr(VI) concentration was quantified using a UV-visible spectrophotometer with diphenylcarbazide colorimetry at 540 nm.[5] A 50-mL volumetric flask combined the diluted Cr(VI) sample solution, 0.5 mL of sulfuric acid solution (1: 1), 0.5 mL of phosphoric acid solution (1: 1), and 2 mL of diphenylcarbazide solution. The particulate Cr concentration was obtained by deducting the concentration of total soluble Cr from total Cr. Similarly, the amount of soluble Cr(III) was obtained by subtracting the concentrations of Cr(VI) from total soluble Cr.

Total Fe (after acid digestion) and total soluble Fe concentrations were analyzed using an inductively coupled plasma atomic emission spectrometer (ICP-MS). The dissolved Fe(II) concentration was detected by phenanthroline spectrophotometry at 510 nm using the UV-visible spectrophotometer.[6] The diluted Fe(II) samples were added to a mixture of 0.4 mL of HCl solution (1: 1), 2 mL of acetic acid-ammonium acetate buffer solution, and 0.5 mL of 1,10-phenanthroline solution (0.12%) in a 10 mL volumetric flask. The particulate Fe concentration was calculated as the difference between the total Fe and the total soluble Fe in the solution.

The concentrations of Fe or Cr species in the retentates (for retention profiles) were obtained from column dissection experiments, similar to our previous studies.[7] The sand in the column was divided into 7 equal parts from top to bottom and then transferred into seven beakers. Dilute HCl and HNO_3 were added to digest nanoparticles on the sand using a plate heater at 220 ℃ until there were no black

particles (nZVI@GT composites). The resulting solution was used for determination after passing through a 0.45 μm filter membrane.

Text S4: Pretreatment of column transport experiment

For the column transport experiments, the quartz sand used as the porous medium was washed with NaOH and HCl solutions (24 h) to remove surface impurities before packing the columns. Then, sand was dried and sieved to ensure grain sizes ranging from 417 to 600 μm. A glass chromatography column (length = 20 cm; inner diameter = 2.6 cm) was used for column experiments. To ensure that the pore volume (PV) in the sand columns was approximately the same for each test, the columns were uniformly filled with a total mass of approximately 150 g of quartz sand with a porosity of 0.467. The PV was calculated using the following formula:

$$PV = \left(\frac{d}{2}\right)^2 \pi h - \frac{M}{\rho}$$

where d was the inner diameter of the column (2.6 cm); h was the filling height of the sand medium in column (20 cm); M was the total mass of the quartz sand (150 g); ρ was the density of quartz sand (2.65 g cm^{-3}).

The calculation formula for the packing density ρ′ was:

$$\rho' = \frac{M}{V} = \frac{M}{(\frac{d}{2})^2 \pi h}$$

where V was the package volume (cm^3).

The calculation formula for the filling porosity θ was:

$$\theta = \frac{PV}{\left(\frac{d}{2}\right)^2 \pi h}$$

To prevent quartz sand from blocking the inlet and outlet, 150 μm nylon membranes (purchased from Millipore) and polytetrafluoroethylene caps were installed at both ends of the column. The

physical conditions of transport columns can be referred to our previous studies.[8]

Text S5: Two-site kinetic attachment model

On the basis of previous studies, the two-site kinetic attachment model has been successfully simulated the transport and retention of particles in porous media:[9, 10]

$$\frac{\partial \theta c}{\partial t} + \rho_b \frac{\partial (s_1)}{\partial t} + \rho_b \frac{\partial (s_2)}{\partial t} = \frac{\partial}{\partial x}(\theta D \frac{\partial c}{\partial x}) - \frac{\partial qc}{\partial x}$$

where ρ_b is defined as the bulk density of the porous matrix [M L^{-3}]; θ is the volumetric water content (dimensionless); c is GT-nZVI colloid concentration in the aqueous phase [N L^{-3}]; t is the time [T]; x is the vertical spatial coordinate [L]; D is the hydrodynamic dispersion coefficient (L_2 T^{-1}); q is the pore water velocity (L T^{-1}). Here, the dispersivity (D) and water rate (q) and were obtained by fitting the concentration data of a conservative tracer solution for the standard convection-dispersion equation with the STANMOD software.[11] s_1 and s_2 are described as the solid phase concentrations on Site 1 and Site 2, respectively. The first kinetic site (Site 1) assumes to be reversible, whereas the second kinetic site (Site 2) assumes to be irreversible and the depth-dependent retention. Where k_1 and k_{1d} are the first-order coefficients on Site 1 for retention and detachment, respectively. And k_2 is the first-order straining coefficient on Site 2.

$$\rho_b \frac{\partial (s_1)}{\partial t} = \theta \psi_t k_1 c - \rho_b k_{1d} s_1$$

$$\rho_b \frac{\partial (s_2)}{\partial t} = \theta k_2 \psi_x c$$

$$\Psi_x = (\frac{d_c + z}{d_c})^{-\beta}$$

The transport parameters (k_1, k_{1d}, and k_2) for the BTCs of nZVI@GT obtained through column experiments are fitted using the HYDRUS-1D code and optimized by a nonlinear least square.

Text S6: Characterization of synthesized M-nZVI@GT and K-nZVI@GT

Fig. S2 presents SEM images of Mont, Kaolin, M-nZVI@GT, and K-nZVI@GT. Analogous to our studies,[1] the spherical nZVI@GT particle was prone to forming larger agglomerates. It can be observed that iron nanoparticles were uniformly distributed on the surface of Mont and Kaolin (Fig. S2b, e). The single-layer structured M-nZVI@GT has better dispersion and smaller particle size than lamellar structured K-nZVI@GT. Regarding the elemental composition of clay-supported nZVI@GT, a strong peak of Fe element contributed to nZVI in composites (Fig. S2c, f). The C and O elemental peaks were mainly attributed to the polyphenol groups in tea polyphenols. In addition, the Al and Si peaks were mostly from Mont and Kaolin minerals, which proved the successful synthesis of the clay-mediated nZVI@GT composites.

The X-ray diffraction spectra of synthesized M-nZVI@GT and K-nZVI@GT are shown in Fig. S3a, b. The diffraction peaks located at $2\theta = 25°$ and $2\theta = 44.9°$ correspond to the characteristic peaks of tea polyphenols and α-Fe^0,[12] respectively. These suggest that organically encapsulated zero-valent iron was prepared during synthesis, which agreed with previous studies. The characteristic peaks of Mont, Kaolin were visible at $2\theta = 19.9°$, 26.8°, 30.1°, 35.4°, 62.0°,[13] and 21.0°, 26.6°, 36.2°, 60.7°, 67.1°,[14] respectively. Partial absorption peaks of Mont and Kaolin were still visible in the synthesized M-nZVI@GT and K-nZVI@GT, which proved the successful loading of iron nanoparticles on clay.

Fig. S3c, d displayed the FTIR spectra of Mont, Kaolin, M-nZVI@GT, and K-nZVI@GT. The spectra showed a large number of absorption peaks between 1800 cm^{-1} and 1000 cm^{-1} on the surface of synthesized composites. The -C=O group (1703 cm^{-1}), C=O&C=C group (1615 cm^{-1}), -CH_2- group (1519 cm^{-1}), -CH_3 group (1468 cm^{-1}), C-H group (1367 cm^{-1}), and C-O group (1094 cm^{-1} and 1043 cm^{-1}) were included. These functional groups were associated with green tea extracts.[15] The Fe-O peak at 612 cm^{-1} was observed for both composites, suggesting the synthesis of tea polyphenol-coated iron nanoparticles. Moreover, the absorption peaks in Mont at 475 cm^{-1}, 520 cm^{-1}, and 844 cm^{-1}

corresponding to Si-O-Si, Si-O-Al (octahedral), and Al-Mg-OH bending vibrations,[13] respectively, were still visible in the M-nZVI@GT's IR spectra. Additionally, K-nZVI@GT and Kaolin also have similar absorption peaks at 475 cm^{-1} (Si-O-Si) and 564 cm^{-1} (Si-O-Al).[14] This indicated that the nZVI@GT particles were successfully loaded on the clay surface, and the clay material maintained its intrinsic chemical composition.

To gain further insight into the suspension stability of the clay-modified nZVI@GT composites, we conducted a study investigating the corresponding particle size changes of M-nZVI@GT and K-nZVI@GT over time (Fig. S9). Both two composites exhibited a relatively stable phase, with M-nZVI@GT displaying a smaller particle size. This could be attributed to the fact that the negative ZPs of M-nZVI@GT are stronger than those of K-nZVI@GT (Fig. 5), which facilitates the dispersion of M-nZVI@GT particles in NaCl solution. Two clay-mediated composites are more stable in solution than nZVI@GT, which is likely due to the incorporation of clay.

References:

1. H. Yang, Z. Ye, F. Feng, N. Xu, J. Yang, Z. Yao, Z. Li and J. Chen, Green-synthesized nanosize Mont-supported Fe0 via tea extract for enhanced transport and in situ remediation of Pb(II) in soil, *J. Soils Sediments.*, 2021, **21**, 2540-2550.
2. C. Zhang, C. L.-C. Suen, C. Yang and S. Y. Quek, Antioxidant capacity and major polyphenol composition of teas as affected by geographical location, plantation elevation and leaf grade, *Food Chem.*, 2018, **244**, 109-119.
3. G. Vilardi, M. Parisi and N. Verdone, Simultaneous aggregation and oxidation of nZVI in Rushton equipped agitated vessel: Experimental and modelling, *Powder Technol.*, 2019, **353**, 238-246.
4. S. Machado, J. P. Grosso, H. P. A. Nouws, J. T. Albergaria and C. Delerue-Matos, Utilization

of food industry wastes for the production of zero-valent iron nanoparticles, *Sci. Total Environ.*, 2014, **496**, 233-240.

5. P. Larese-Casanova and M. M. Scherer, Abiotic Transformation of Hexahydro-1,3,5-trinitro-1,3,5-triazine (RDX) by Green Rusts, *Environ. Sci. Technol.*, 2008, **42**, 3975-3981.
6. Q. Shao, C. Xu, Y. Wang, S. Huang, B. Zhang, L. Huang, D. Fan and P. G. Tratnyek, Dynamic interactions between sulfidated zerovalent iron and dissolved oxygen: Mechanistic insights for enhanced chromate removal, *Water Res.*, 2018, **135**, 322-330.
7. Z. Ye, N. Xu, D. Li, J. Qian, C. Du and M. Chen, Vitamin C mediates the activation of green tea extract to modify nanozero-valent iron composites: Enhanced transport in heterogeneous porous media and the removal of hexavalent chromium, *J. Hazard. Mater.*, 2021, **411**, 125042.
8. Y. Feng, N. Xu, L. Peng, J. Shen and X. Yang, Nano-size plastics inhibited Cr(VI) species transformation during facilitated transport of green synthesized nano-iron in the presence of oxyanions, *J. Hazard. Mater.*, 2023, **456**, 131716.
9. S. A. Bradford, J. Simunek, M. Bettahar, M. T. van Genuchten and S. R. Yates, Modeling colloid attachment, straining, and exclusion in saturated porous media, *Environ. Sci. Technol.*, 2003, **37**, 2242.
10. J. F. Schijven and J. Šimůnek, Kinetic modeling of virus transport at the field scale, *J. Contam. Hydrol.*, 2002, **55**, 113-135.
11. J. Šimůnek, M. T. van Genuchten and M. Šejna, Development and Applications of the HYDRUS and STANMOD Software Packages and Related Codes, *Vadose Zone J.*, 2008, **7**, 587-600.
12. T. Wang, X. Jin, Z. Chen, M. Megharaj and R. Naidu, Green synthesis of Fe nanoparticles using eucalyptus leaf extracts for treatment of eutrophic wastewater, *Sci. Total Environ.*, 2014,

466-467, 210-213.

13. P. Wu, Y. Dai, H. Long, N. Zhu, P. Li, J. Wu and Z. Dang, Characterization of organo-montmorillonites and comparison for Sr(II) removal: Equilibrium and kinetic studies, *Chem. Eng. J.*, 2012, **191**, 288-296.
14. X. Zhang, S. Lin, Z. Chen, M. Megharaj and R. Naidu, Kaolinite-supported nanoscale zero-valent iron for removal of Pb2+ from aqueous solution: Reactivity, characterization and mechanism, *Water Res.*, 2011, **45**, 3481-3488.
15. W. Sun, N. Xu, W. Jiang and G. Cheng, Mechanistic insights into manganese oxide impacting the oxidation and transport of Cr(III) immobilized by nano-zero valent charged ion particles in water-saturated porous media, *J. Hazard. Mater.*, 2024, **469**, 134050.
16. C. Zhou, C. Han and N. Liu, Critical layer in liquid-solid system influencing the remediation of chromium using zeolite-supported sulfide nano zero-valent iron, Journal of Environmental Sciences, 2024, **135**, 232-241.
17. T. Liu, Z.-L. Wang, X. Yan and B. Zhang, Removal of mercury (II) and chromium (VI) from wastewater using a new and effective composite: Pumice-supported nanoscale zero-valent iron, *Chemical Engineering Journal*, 2014, **245**, 34-40.
18. Y. Li, Z. Jin, T. Li and Z. Xiu, One-step synthesis and characterization of core–shell Fe@SiO_2 nanocomposite for Cr (VI) reduction, Science of The Total Environment, 2012, **421-422**, 260-266.
19. C. Mystrioti, T. D. Xanthopoulou, P. Tsakiridis, N. Papassiopi and A. Xenidis, Comparative evaluation of five plant extracts and juices for nanoiron synthesis and application for hexavalent chromium reduction, Science of The Total Environment, 2016, **539**, 105-113.

Table S1. Transport percentage of different Cr species in the effluent when M-nZVI@GT and K-nZVI@GT cotransport with Cr(VI) in the presence of phosphate or HA.

Experimental condition		Soluble Cr(VI) (%)	Soluble Cr(III) (%)	Particulate Cr (%)
M-nZVI@GT with Cr(VI)	Control	49.05	17.81	28.87
	With P	64.63	7.88	24.49
	With HA	71.16	5.19	22.55
K-nZVI@GT with Cr(VI)	Control	65.51	12.89	18.57
	With P	77.49	7.70	13.42
	With HA	71.67	9.49	14.65

Table S2. Mass recovery of total Fe and total Cr in the effluent and sand columns during transport of M-nZVI@GT and K-nZVI@GT with Cr(VI) under different experimental conditions.

Experimental condition		Transport (%)		Retention (%)		Total (%)	
		Fe	Cr	Fe	Cr	Fe	Cr
M-nZVI@GT with Cr(VI)	Control	41.03	95.73	56.12	2.06	97.15	97.79
	With P	52.20	97.00	43.13	2.98	95.33	99.98
	With HA	49.86	98.90	48.78	1.46	98.64	100.36
K-nZVI@GT with Cr(VI)	Control	37.56	96.97	59.43	2.27	96.99	99.24
	With P	47.47	98.60	52.36	1.48	99.83	100.08
	With HA	43.75	95.81	54.52	2.84	98.27	98.65

Table S3. Components and corresponding relative percentage of Fe 2p and Cr 2p XPS spectra for M-nZVI@GT and K-nZVI@GT after reaction with Cr(VI) in the presence of phosphate or HA.

Components		Binding Energy (eV)	Relative Percentage (%) of M-nZVI@GT with Cr(VI)			Relative Percentage (%) of K-nZVI@GT with Cr(VI)		
			Control	W. P	W. HA	Control	W. P	W. HA
Fe 2p	FeO	710.6	47.20	34.11	38.66	40.26	23.20	34.40
	Fe_2O_3	712.4	25.28	36.19	26.17	34.75	41.51	27.98
	Fe(II) Satellite	714.5	27.52	29.70	35.17	24.99	35.29	37.62
Cr 2p	Cr_2O_3	576.9	45.53	29.60	43.61	45.14	29.98	38.09
	$Cr(OH)_3$	577.9	38.24	46.77	30.34	32.12	40.77	36.21
	Cr(VI)	579.3	16.23	23.63	26.05	22.74	29.25	25.70

Table S4. Removal capacity of Cr(VI) by different types of nZVI nanocomposites.

Types of nZVI	Synthesis method	Capacity (mg Cr(VI)/g Fe)	Reference
Z/S-nZVI	methods: borohydride synthesis ($NaBH_4$) modifier: ZSM-5 zeolite	294.92	16
P-NZVI	methods: borohydride synthesis ($NaBH_4$) modifier: pumice	306.6	17
Fe@SiO_2	methods: borohydride synthesis (KBH_4) modifier:.tetraethylorthosilicate (TEOS)	467	18
nFe	methods: green synthesis (herb extracts)	500	19
M-nZVI@GT	methods: green synthesis (green tea extracts) modifier: Mont	1026	This work
K-nZVI@GT	methods: green synthesis (green tea extracts) modifier: Kaolin	772	This work

Table S5. Estimated cost for the clay-mediated nZVI@GT material.

Materials	**Amount**	**Price**
$Fe_2(SO_4)_3$	3.333 g	¥1.80
Clay (Mont/Kaolin)	0.111 g	¥0.05
Green tea	12.50 g	¥1.05
Ethanol absolute	250 mL	¥4.00
DI Water	500 mL	¥0.20
Other expenses	——	¥0.75
Total cost of 1g clay-mediated nZVI@GT		**¥7.85**

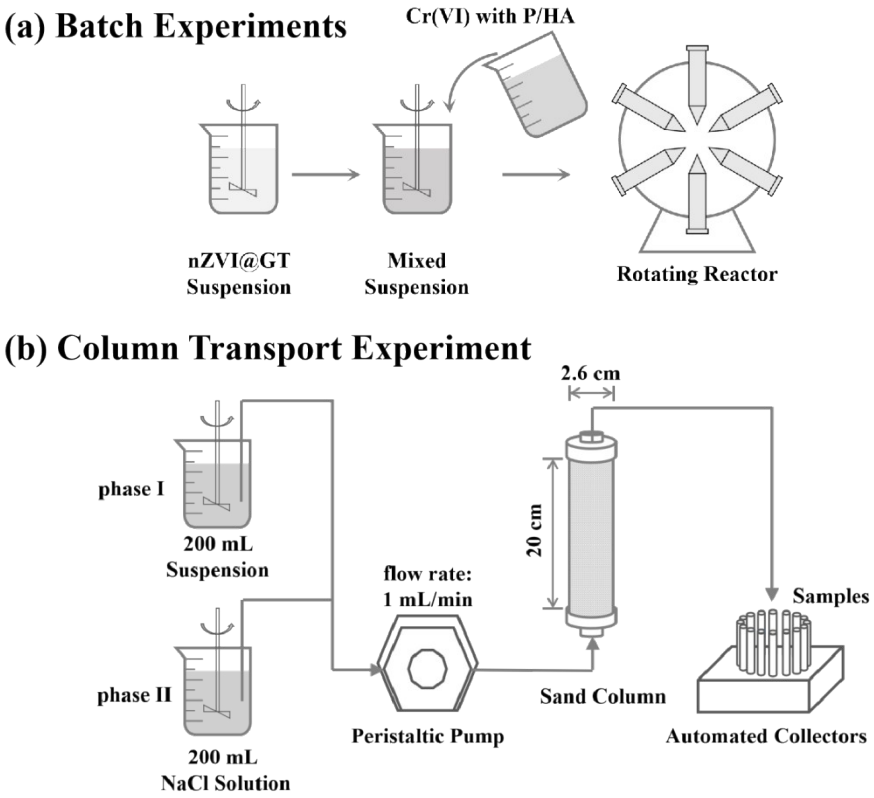

Fig. S1. Experimental set-up diagrams for batch (a) and column transport experiment (b).

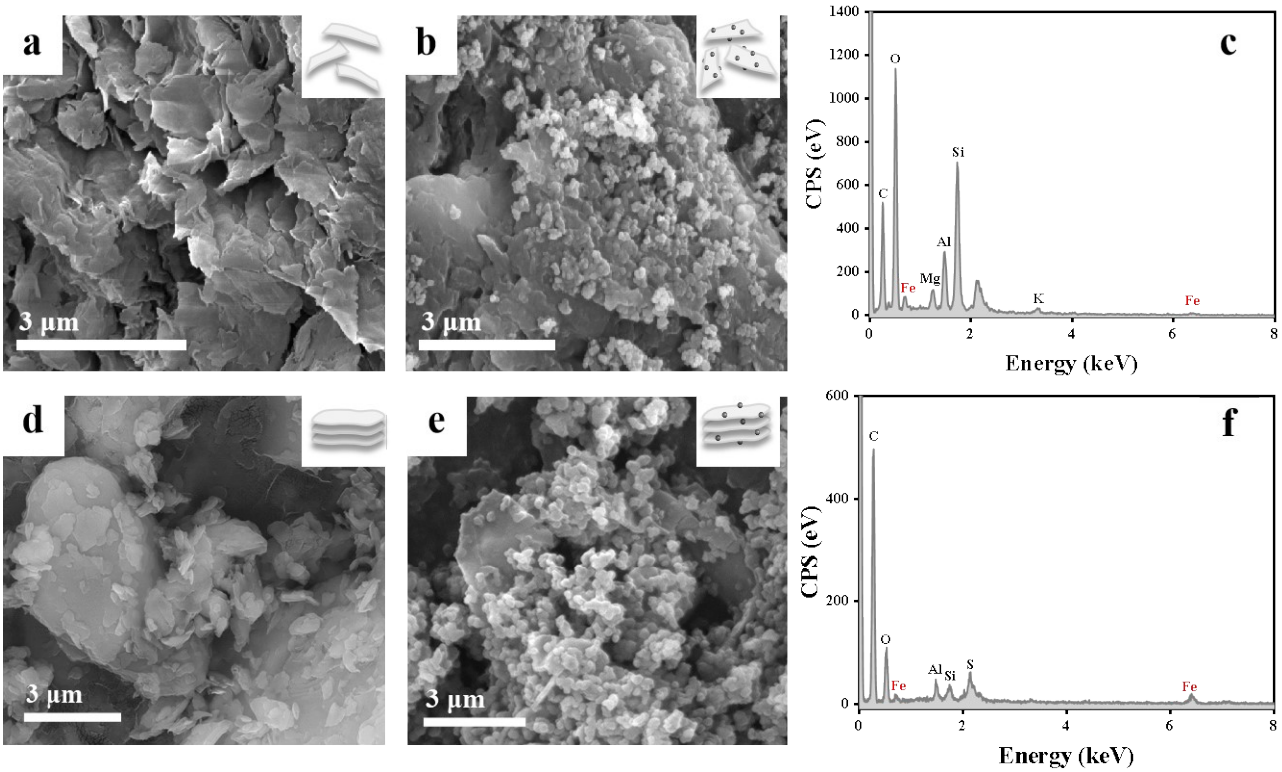

Fig. S2. SEM images of Mont (a), M-nZVI@GT (b), Kaolin (d), K-nZVI@GT (e), and EDS of M-nZVI@GT (c) and K-nZVI@GT (f).

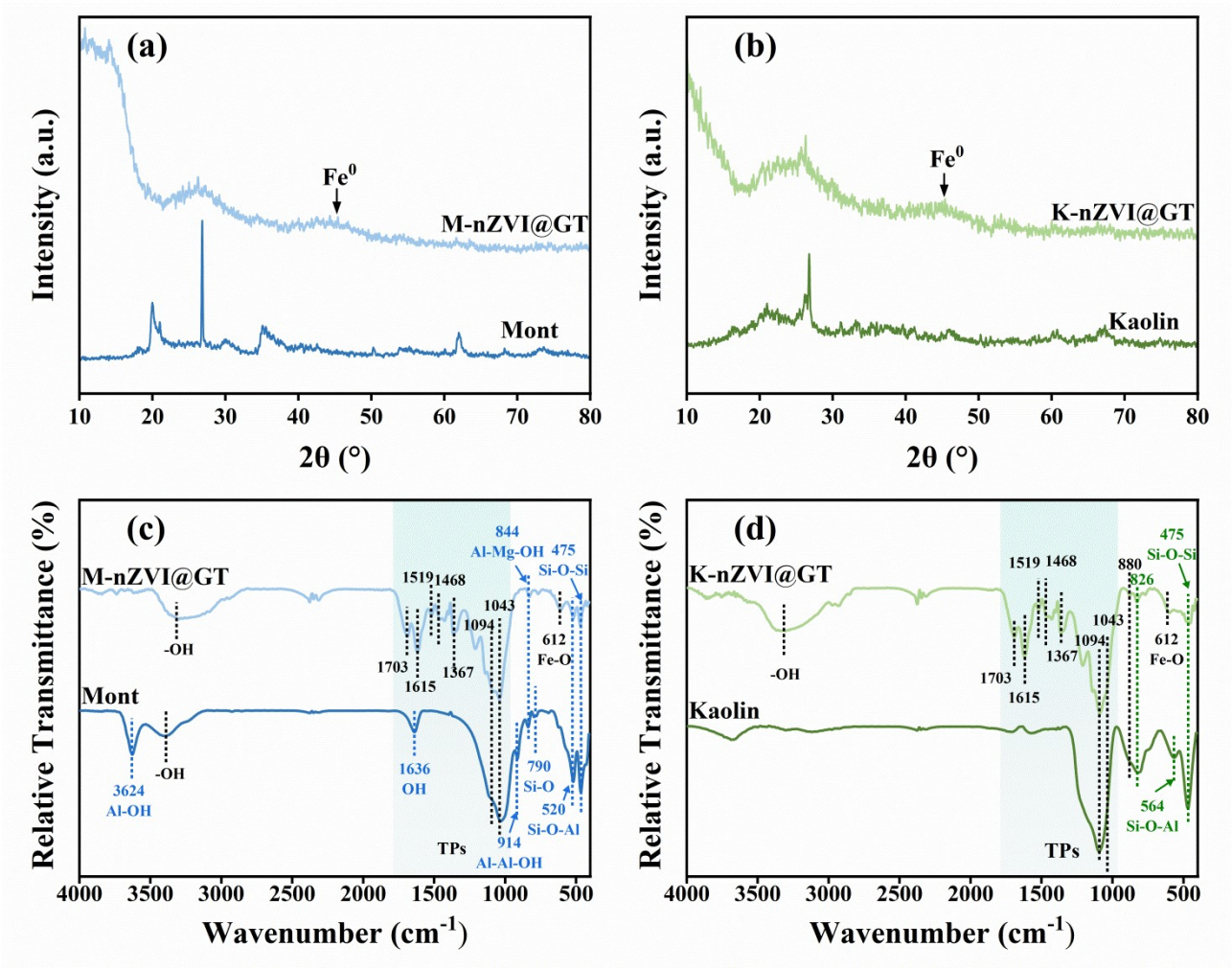

Fig. S3. XRD patterns (a, b) and FTIR spectra (c, d) of Mont, M-nZVI@GT, Kaolin and K-nZVI@GT.

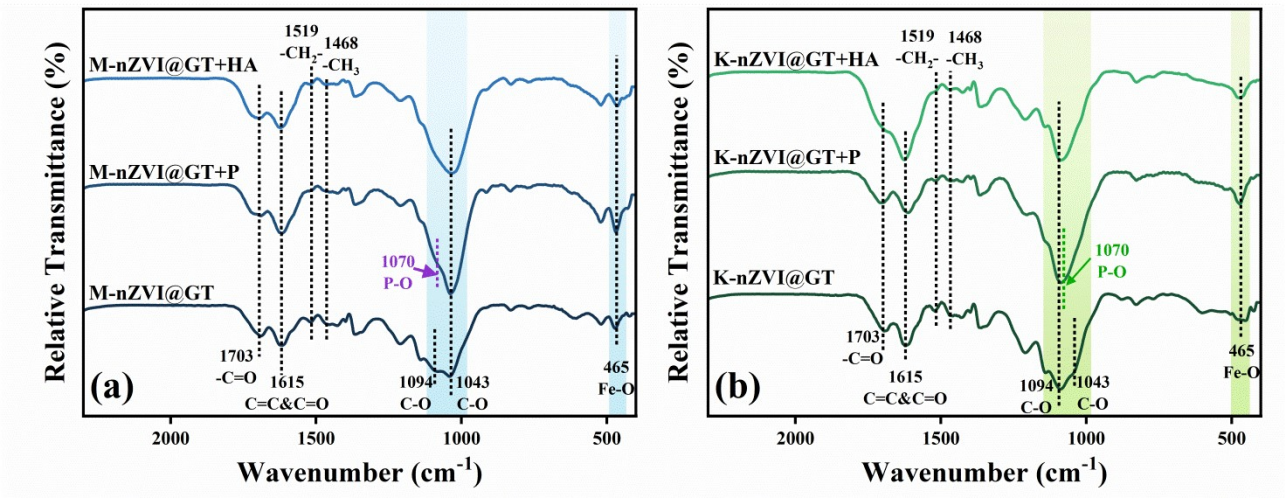

Fig. S4. FTIR spectra of M-nZVI@GT (a) and K-nZVI@GT (b) in the presence of phosphate and HA.

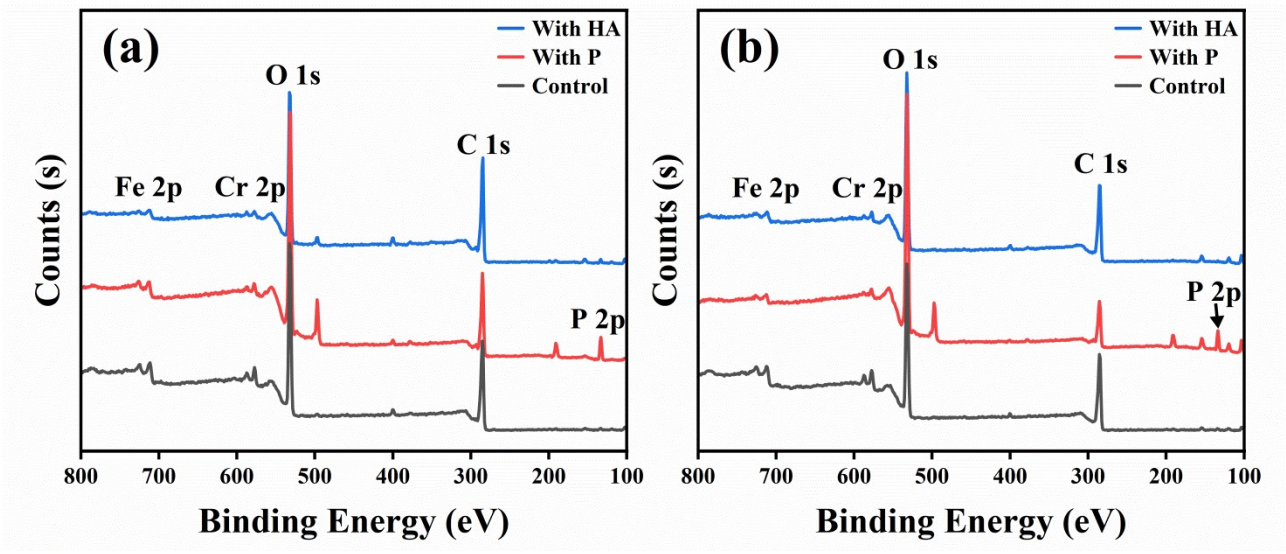

Fig. S5. XPS full scan spectra of M-nZVI@GT (a) and K-nZVI@GT (b) with Cr(VI) in the presence of phosphate and HA.

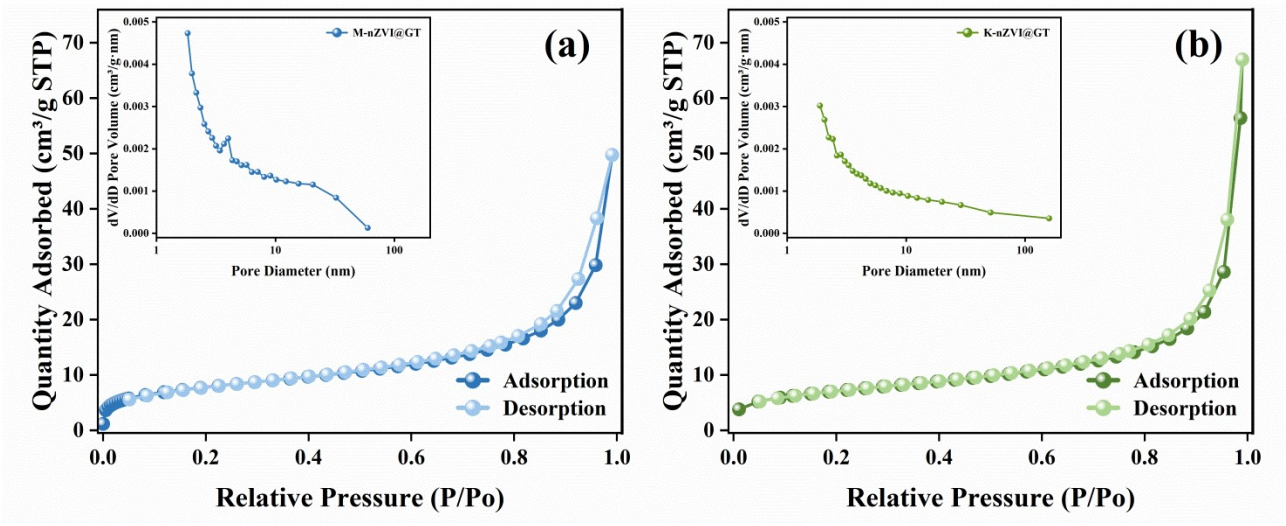

Fig. S6. BET of M-nZVI@GT (a) and K-nZVI@GT (b).

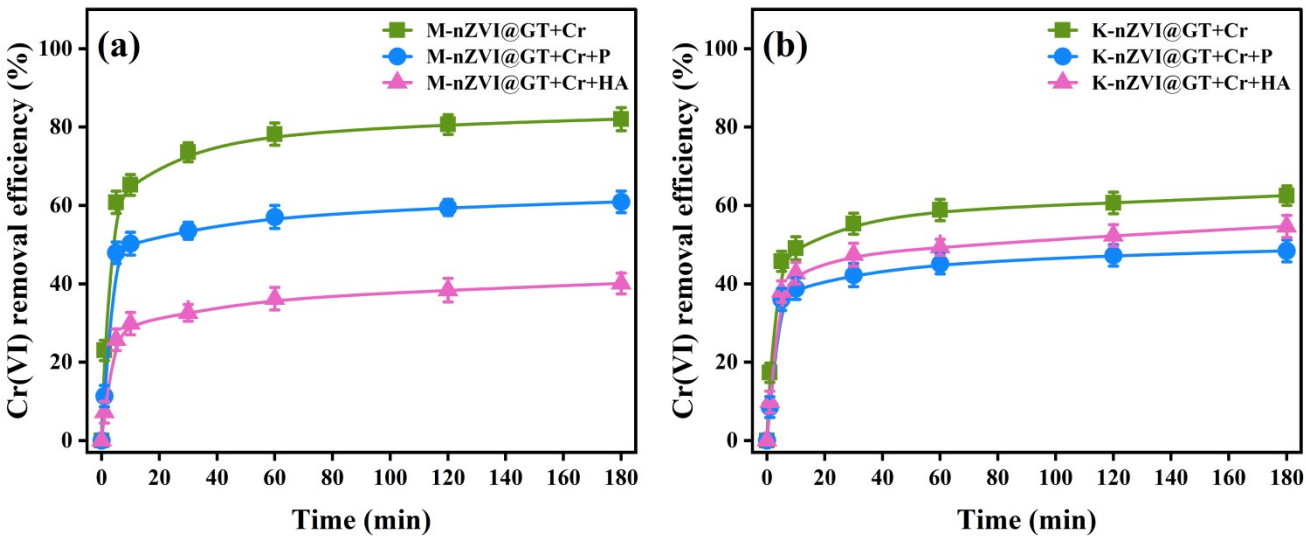

Fig. S7. Cr(VI) removal efficiency of M-nZVI@GT (a) and K-nZVI@GT (b) over time in the presence of phosphate and HA at pH 3.0.

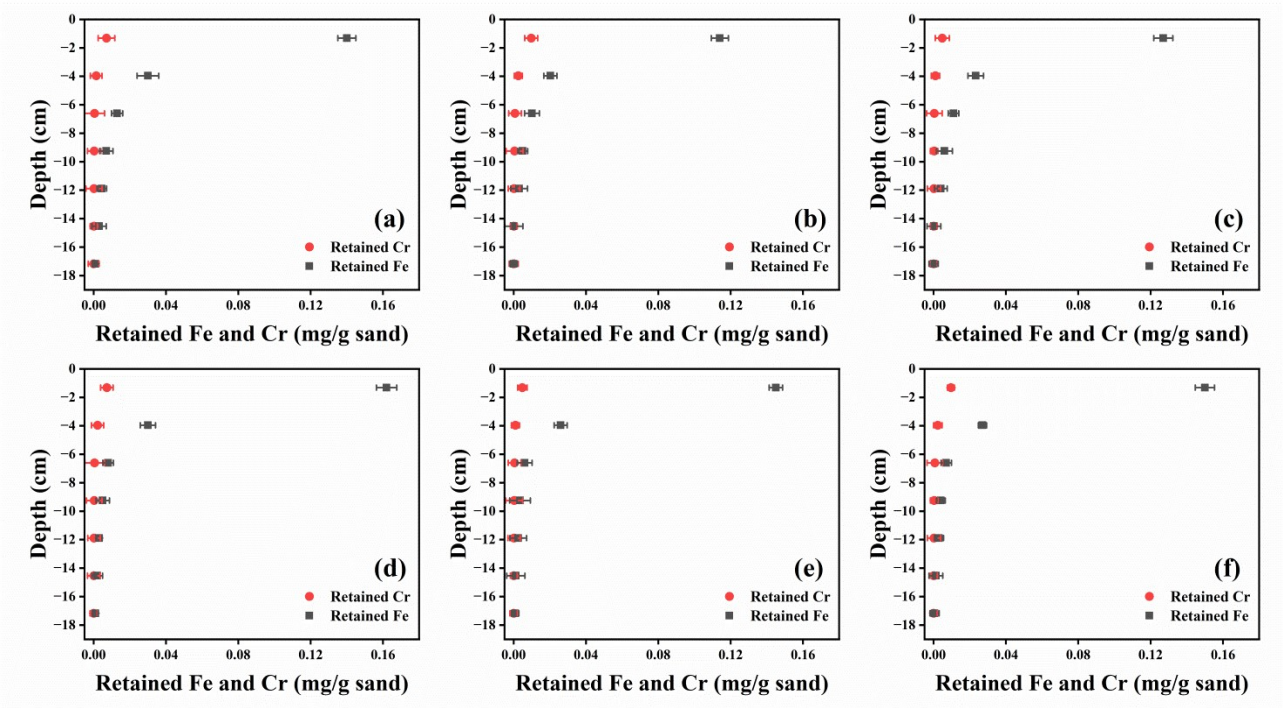

Fig. S8. Retention profiles of M-nZVI@GT (a, b, c) and K-nZVI@GT (d, e, f) (0.5 g·L^{-1}) cotransport with Cr(VI) (50 mg·L^{-1}) in the presence of phosphate (b, e) and HA (c, f) in 1 mM NaCl solution at pH 6.0.

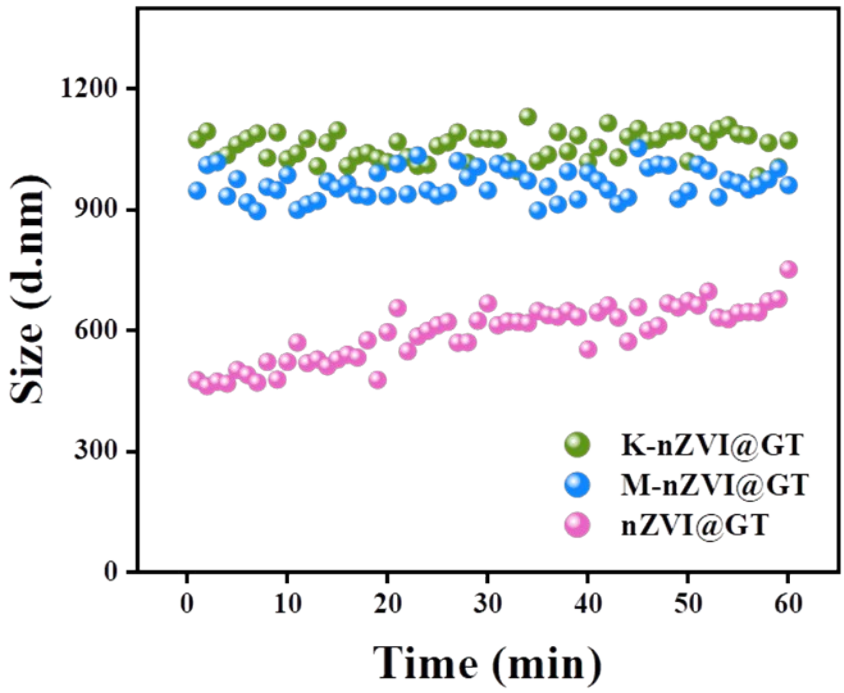

Fig. S9. Suspension kinetics of nZVI@GT, M-nZVI@GT and K-nZVI@GT in 1 mM NaCl at pH=6.0.

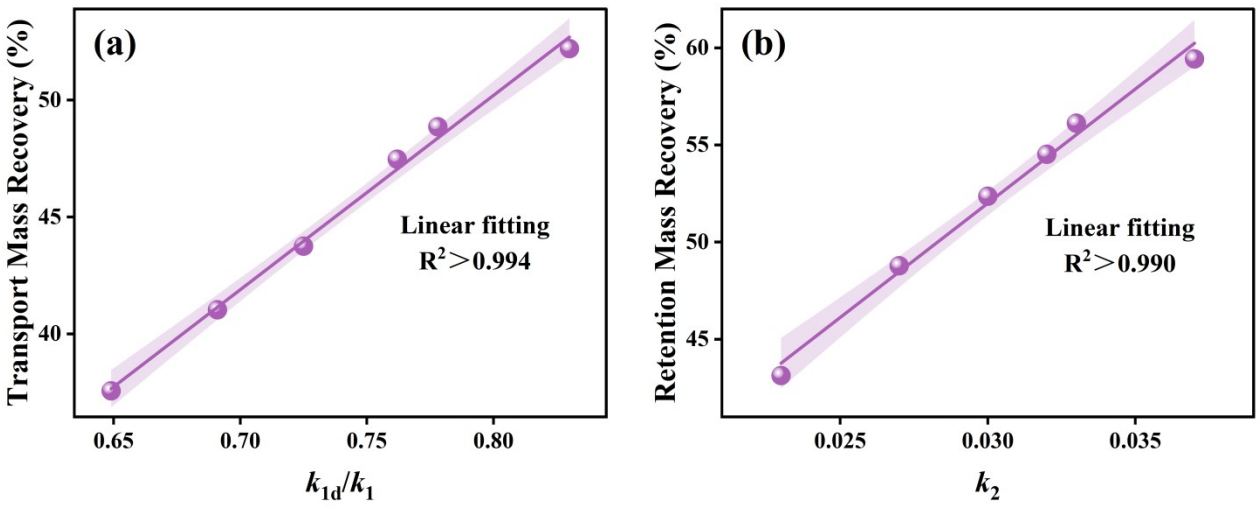

Fig. S10. Correlation between k_{1d}/k_1 values and transport mass recovery of Fe (a) and correlation between k_2 values and retention mass recovery of Fe (b) for clay modified nZVI@GT composites in the presence of phosphate and HA.

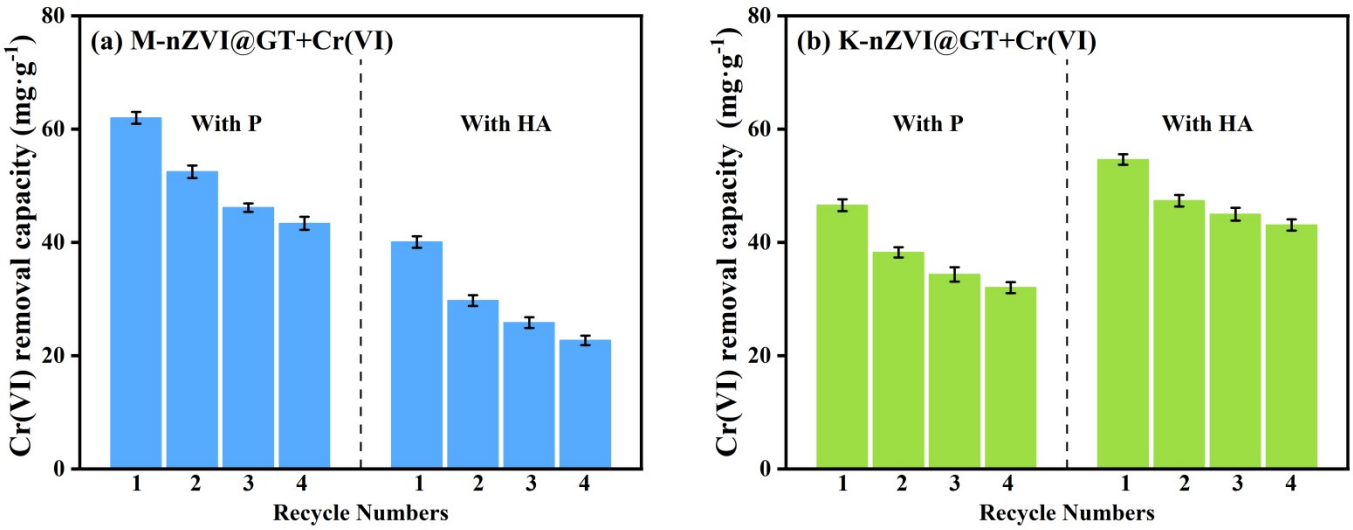

Fig. S11. Recycling for the Cr(VI) removal efficiency of M-nZVI@GT (a) and K-nZVI@GT (b) (0.5 g L^{-1}) in the presence of phosphate and HA at pH 3.0.